Processing and Application of Ceramics 10 [2] (2016) 107–115
DOI: 10.2298/PAC1602107M

Hybrid electrode obtained by sol-gel derived $Ni_{0.3}Co_{2.7}O_4$ nanoparticles incorporated into polypyrrole: Electrocatalysis of O_2 reduction

Mourad Mechouet*, Naima Idiri, Celia Belkessam, Abdelaziz Kadri, Nassima Benbrahim

Laboratoire de Physique et Chimie des Matériaux de l'Université Mouloud Mammeri de Tizi-Ouzou. Route de Hasnaoua BP. 17 RP 15000, Tizi-Ouzou, Algeria

Received 10 March 2016; Received in revised form 16 May 2016; Received in revised form 24 June y 2016; Accepted 27 June 2016

Abstract

A hybrid electrode was formed on glassy carbon (GC) electrode with polypyrrole (PPy) and mixed valence $Ni_{0.3}Co_{2.7}O_4$ nanoparticles to study their behaviour towards the oxygen reduction reaction (ORR). The oxide nanoparticles were prepared by sol-gel route using various parameters and characterized by XRD, SEM, EDX and BET methods. The result showed that desired oxide was obtained and nanocrystallites exhibit a specific surface area ranging from 39 to 73 m^2/g with diameter varying from 13 to 25 nm. The hybrid electrode was then fabricated by electropolymerization of pyrrole (Py) in the presence of the smallest $Ni_{0.3}Co_{2.7}O_4$ nanoparticles in KCl (0.15 mol/L) at room temperature and characterized by EDX, SEM and LSV methods. Investigation of the hybrid electrode confirmed that O_2 reduction mechanism changes by applying potential. Thus, at low overpotential the O_2 reduction involves two electrons and provides H_2O_2, with cathodic transfer coefficients (β) of 0.33 and exchange current density (j_0) of about 8×10^{-3} mA/cm^2, while, at high overpotential H_2O_2 is further reduced into H_2O. The results also show that sol-gel method led to the preparation of $Ni_{0.3}Co_{2.7}O_4$ nanoparticles having a spinel structure with a desired stoichiometry which exhibits a high electrocatalytic activity for reducing oxygen mostly to H_2O_2.

Keywords: *sol-gel process, nanopowders, composites, catalytic properties, oxygen reduction reaction*

I. Introduction

Over the last years electrocatalyst particles dispersion throughout the matrix of an electronically conductive polymer (ECP) as electrocatalytic systems for various reactions were widely explored [1–5]. Thus, the obtained composite exhibits a three-dimensional distribution of accessible active sites and provides a better charge transport conditions through the polymer film [6].

Among ECP, polypyrrole (PPy) has attracted a great attention in recent years due to its non-toxicity [7], easy fabrication by electropolymerization (which promotes application of aqueous and organic solvents and using chemical and electrochemical methods) [8], high conductivity [9], thermal and environmental stability [10,11]. Several recent studies focused on the development of a composite electrode for oxygen reduction reaction (ORR) catalysis and production of H_2O_2 [12], which can be used as an oxidizer of organic pollutants and bleaching or sterilizing agent in chemical or pharmaceutical industry [13]. The spinel $Ni_xCo_{3-x}O_4$ ($0 \leq x \leq 1$) nanoparticles seem to be very promising electrocatalyst. Thus, Chartier *et al.* [14,15] reported that the nanoparticles with $x = 0.3$, synthesized by thermal decomposition of nitrates, had the average size of 35 nm and maximum O_2 reduction activity producing high amount of H_2O_2, with an exchange current density (j_0) of 2×10^{-3} mA/cm^2.

Many authors claimed [16,17] that when the catalysts dimensions are reduced, the materials properties might be remarkably changed. It was noticed that the preparation route influences the oxide physicochemical properties [18], including its size [19,20]. Among dif-

* Corresponding author: tel: +213 665 651253,
fax: +213 26 111527, e-mail: *mechouetmourad@yahoo.fr*

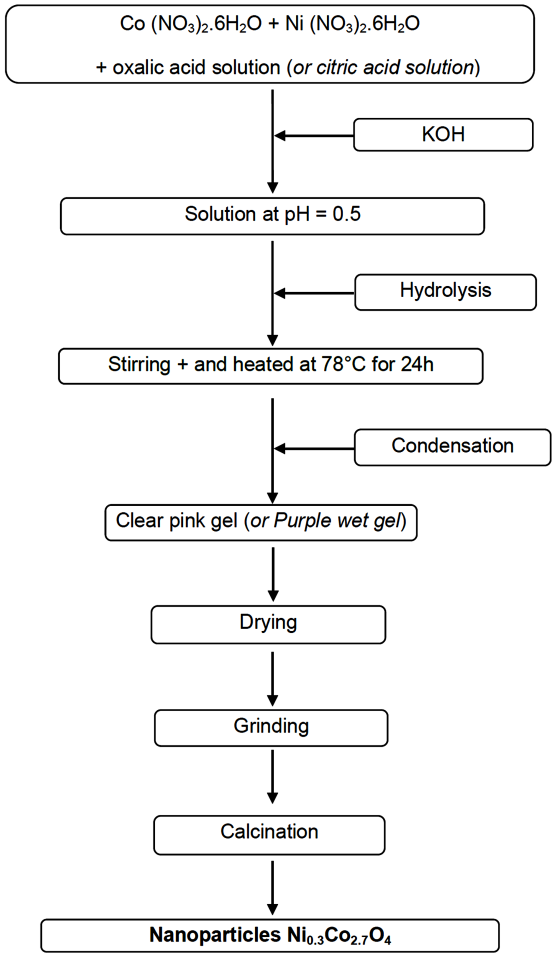

Figure 1. Scheme of sol-gel synthesis of $Ni_{0.3}Co_{2.7}O_4$ nanoparticles with oxalic acid and citric acid as chelating agents

ferent synthesis methods, sol-gel is considered as a low-temperature soft chemical route [21] frequently used to produce nanosized oxide powders [22] having a strong catalytic activity and relatively high stability [23].

In this study, different $Ni_{0.3}Co_{2.7}O_4$ powders were prepared by sol-gel method using two chelating agents (oxalic/citric acids) and different calcination temperatures (300/350 °C). Electrocatalytic activity of the embedded oxide particles in polypyrrole film (being part of a sandwich hybrid electrode GC/PPy/PPy($Ni_{0.3}Co_{2.7}O_4$)/PPy) has been studied. In order to improve this interesting property, $Ni_{0.3}Co_{2.7}O_4$ powder with the smallest particles was selected. The sandwich hybrid electrode was characterized by linear sweep voltammetry (LSV) using rotating disc electrode (RDE) [23]. The data were exploited by Koutecky-Levich (K-L) equation to evaluate ORR kinetic parameters that allow us to check out the electrocatalytic performances.

II. Experimental

Nanocrystalline $Ni_{0.3}Co_{2.7}O_4$ powders were synthesized by sol-gel method using nickel and cobalt nitrates and two different chelating agents. The powder with the smallest particles was then dispersed in PPy matrix (to form PPy($Ni_{0.3}Co_{2.7}O_4$) film) and sandwiched between two PPy layers, leading to the formation of hybrid electrode [GC/PPy/PPy($Ni_{0.3}Co_{2.7}O_4$)/PPy] used for the investigation of its oxygen reduction ability.

2.1. Preparation of $Ni_{0.3}Co_{2.7}O_4$

Precursor nitrate solution, having Co and Ni cation ratio 9:1, was prepared by mixing cobalt (II) nitrate ($Co(NO_3)_2 \times 6\,H_2O$) and nickel (II) nitrate ($Ni(NO_3)_2 \times 6\,H_2O$) salts. Two chelating agents (oxalic and citric acids) were separately added to the nitrates mixture and stirred for 24 h under air at 25 °C. Oxalic and citric acids were dissolved in ethanol (95.0%), and distilled water, respectively. The pH value of the nitrate mixtures was adjusted to 0.5 by carefully adding small amount of KOH solution. Two solutions were then stirred for 10 h, heated at 78 °C until formation of wet gels is observed. Subsequently, wet gels were dried at 100 °C, hand ground to a fine powder with an agate mortar and pestle and finally heat treated at 300 °C or 350 °C for 2 h. The synoptic schemes of both approaches are shown in Fig. 1.

2.2. Powder characterization

Phase purification of the as-prepared products was analysed by X-ray powder diffraction (XRD) with an X-ray diffractometer D008 Siemens using $Cu_{K\alpha}$ radiation λ = 1.5418 Å. XRD profiles were measured in the 2θ range 10–90°, using a scan rate of 0.05° and collection time of 10 s. Plane indexation was realized in agreement with data of the ASTM power diffraction file. The unit cell parameter a was evaluated using a least-squares program on basis of observed inter-planar d spacing and Miller indexes hkl. The specific surface area of the powders (S_p) was measured by nitrogen adsorption at 77.3 K using a Micromeritics ASAP 2010 gas sorption analyser and estimated by the BET equation. Morphology and composition of the synthesized powders were characterized with SEM and EDX, recorded using Siemens XL30 equipment.

2.3. Preparation of composite electrode

The composite electrode, consisting of three layers (GC/PPy, PPy($Ni_{0.3}Co_{2.7}O_4$) and PPy), was prepared in three consecutive steps, which will be described below.

Preparation of GC/PPy: Electropolymerization of pyrrole (Py, Aldrich) was carried out in a classical electrochemical cell. The working electrode was a glassy carbon (GC) rotating disk with a cross-section area of 0.2 cm^2. The counter electrode was a platinum plate of 1 cm^2 area. The reference electrode was a saturated Ag/AgCl electrode. Pyrrole (Py) was purified by distillation to remove oligomers and oxidized forms constantly present in the as-received product. The PPy film was deposited on GC electrode from a solution containing 0.1 mol/L of Py and 0.15 mol/L KCl at room temperature. Prior every trial, the solution was deaer-

ated by nitrogen bubbling for 30 min and maintained under it during the whole experiment. Electrodeposition was performed with a constant current density of 1 mA/cm^2 during 60 s using a Potentiostat/Galvanostat Autolab PGSTAT 30 driven by FRA 4.9 Software and controlled by a PC. The same equipment and software were used for all electrochemical experiments.

Preparation of GC/PPy/PPy($Ni_{0.3}Co_{2.7}O_4$): The prepared GC/PPy was immersed in a solution containing 0.1 mol/L Py, 0.15 mol/L KCl and 7 g/L $Ni_{0.3}Co_{2.7}O_4$. The nanoparticles were incorporated in PPy layer during the galvanostatic electropolymerization process with a current density of 1 mA/cm^2 during 150 s, and the composite thin film was obtained.

Preparation of GC/PPy/PPy($Ni_{0.3}Co_{2.7}O_4$)/PPy: The prepared GC/PPy/PPy($Ni_{0.3}Co_{2.7}O_4$) electrode was covered with a protective thin PPy film, which is obtained by electrolysis at 1 mA/cm^2 for 20 s using a solution containing 0.1 mol/L of Py and 0.15 mol/L KCl.

2.4. Characterization of composite electrode

SEM and EDX were used to characterize the modified polymer surface and its composition. The electrochemical characterization was performed at room temperature in KCl (0.15 mol/L) solution. The reduction current was normalized to the GC electrode cross-section area.

2.5. Electrokinetic parameters

The rotating disc electrode (RDE) was used to evaluate electrokinetic parameters of the oxygen reduction reaction (ORR) by performing LSV at different rotational speeds. The aqueous solution was saturated by oxygen throughout the experiment. The obtained data were then analysed by K-L equation:

$$\frac{1}{j} = \frac{1}{j_k} + \frac{1}{0.2 \cdot n \cdot F \cdot C \cdot D^{2/3} \cdot \nu^{-1/6} \cdot \omega^{1/2}} \qquad (1)$$

where j is the measured current density, j_k is the kinetic current density, ω is the electrode rotational speed, n is the transferred electrons number per one oxygen molecule, F is the Faraday constant, C is oxygen bulk concentration (1.2×10^{-6} mol/cm^3) [24], D is oxygen coefficient diffusion (1.76×10^{-5} cm^2/s) [25] and ν is the solution kinematic viscosity (0.01 cm^2/s). The plot of the inverse of the current density at a given potential vs. $\omega^{-1/2}$ gives the inverse of kinetic current density j_k^{-1} and the total number of electrons n as the ordinate intercept at infinite ω and slope, respectively.

The overpotential is related to the kinetic current density according to equation 2:

$$\frac{1}{j_k} = \frac{1}{j_i} + j_0 \exp\left(\frac{\eta}{b}\right) \qquad (2)$$

where j_i is the limiting current density and b is the Tafel constant and can be determined by:

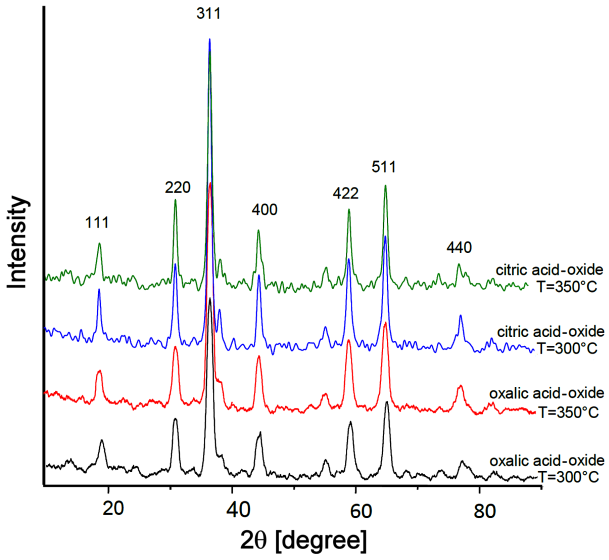

Figure 2. X-ray diffractograms of $Ni_{0.3}Co_{2.7}O_4$ powders prepared with oxalic and citric acids and calcined at 300 and 350 °C

$$b = \frac{R \cdot T}{n \cdot \beta \cdot F} \qquad (3)$$

For high overpotential, j_k^{-1} approaches to j_i^{-1}. In this case, the limiting current can be estimated and then used to calculate the kinetic parameters of ORR (β, j_0) according to equation 4 [26]:

$$\eta = E - E_{eq} = -b \cdot \left(\ln\frac{j_i}{j_0} + \ln\frac{j_k}{j_i - j_k}\right) \qquad (4)$$

Indeed, the plot of η or $E = f(\ln(j_k/(j_i - j_k)))$ gives b, therefore β from the slope and j_0 from the ordinate intercept.

III. Results

3.1. Powder characterization

X-ray diffraction spectra, presented in Fig. 2, confirmed the crystalline nature of the prepared $Ni_{0.3}Co_{2.7}O_4$ nanoparticles. The characteristic *hkl* lines: 111, 220, 311, 400, 422, 511 and 440, indicated on the pure cubic spinel structure. Similar results were obtained by Chartier *et al.* [27] for the powders prepared by thermal decomposition of nitrates. The estimated crystallites cell parameter a is about 8.11 ± 0.015 Å. Some small discrepancies between the experimental a values for different $Ni_{0.3}Co_{2.7}O_4$ powders appeared probably due to the differences between synthesis procedures. However, both synthesis strategies lead to the formation of the pure spinel structure. The crystallites average size $d_{p(XRD)}$ was estimated by Scherrer formula and it was ranging from 13 to 25 nm (Table 1).

The specific surface area of the powders, S_p, was estimated using BET equation and used for determination of particles size $d_{p(BET)}$:

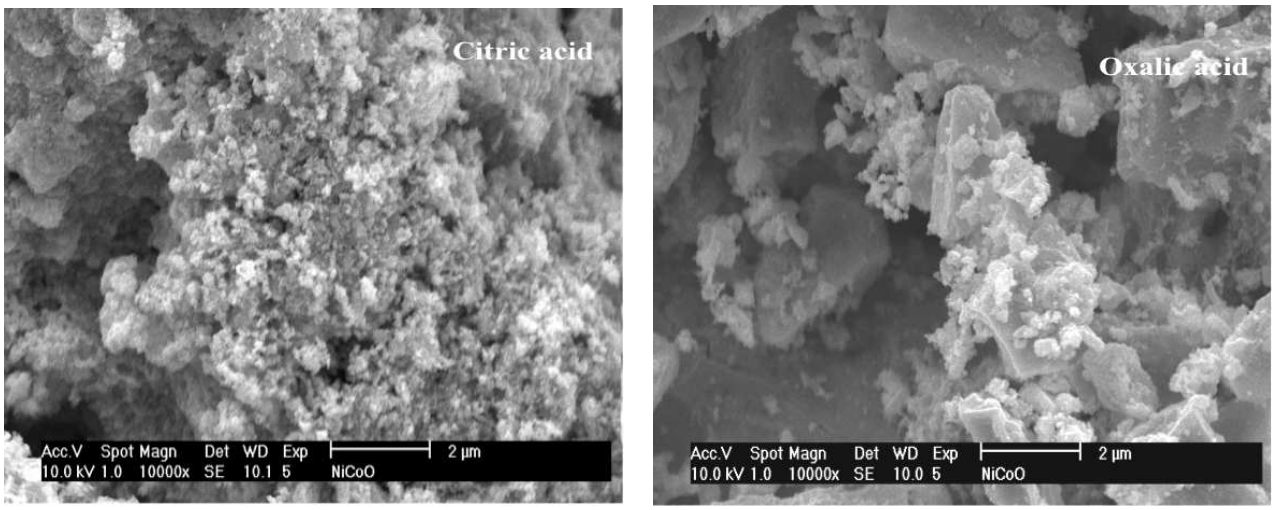

(a) (b)

Figure 3. SEM micrographs of $Ni_{0.3}Co_{2.7}O_4$ powders prepared with oxalic (a) and citric (b) acids and calcined at 300 °C for 2 h

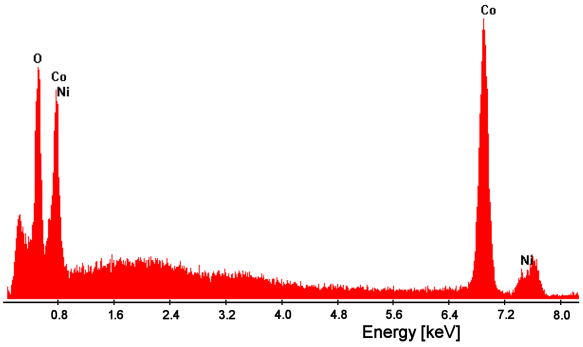

Figure 4. EDX analysis of $Ni_{0.3}Co_{2.7}O_4$ powders synthesised with citric acid and calcined at 350 °C for 2 h

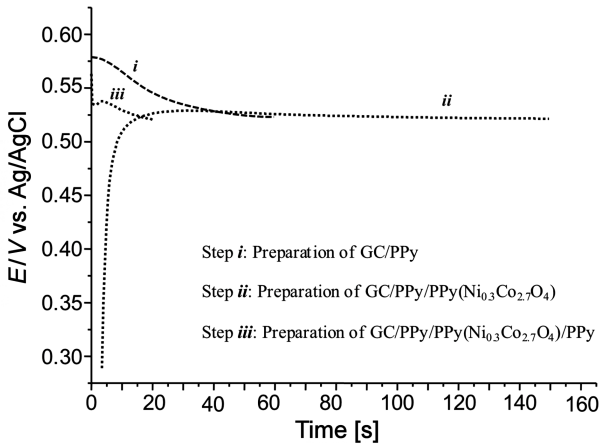

Figure 5. Chronopotentiograms recorded during successive electrodeposition steps

$$d_{p(BET)} = \frac{6}{S_p \cdot \rho_{ox}} \tag{5}$$

where ρ_{ox} is the sample density (7.6 g/cm^3). It can be seen from Table 1 that all four $Ni_{0.3}Co_{2.7}O_4$ powders have fine structure with nanometric particle size, which is even lower than that reported by Chartier *et al.* [27]. The average size of the oxide particles increases while its specific surface area decreases with an increase of calcination temperature. Besides, at a given calcination temperature, somewhat smaller particles were obtained when citric acid was used. Thus, the smallest oxide average size was obtained using citric acid and calcination temperature of 300 °C.

SEM images of the synthesized powders are shown in Fig. 3. It is clear that the obtained $Ni_{0.3}Co_{2.7}O_4$ is constituted of faceted primary nano-crystallites agglomerates. The particles obtained with oxalic acid are less homogeneous than those obtained with citric acid. Composition, i.e. Co and Ni cation ratio, of the powders prepared with oxalic and citric acids and calcined at 350 °C was determined by EDX. As both powders have very similar EDX spectrum, only one was presented in Fig. 4 and the corresponding Co and Ni cation ratios are listed in Table 2. The obtained results suggest that the formed nanopowders exhibit the desired stoichiometry. The same conclusions, from EDX results, were obtained by other authors [27] for the nanopowders synthesized by nitrates thermal decomposition method.

Table 1. Oxide average sizes deduced from BET and XRD analysis

Chelating agent	Oxalic acid		Citric acid	
Calcination temperature [°C]	300	350	300	350
Specific surface area, S_p [m^2/g]	61	39	73	48
Average particle size, $d_{p(BET)}$ [nm]	15	23	14	21
Average crystallite size, $d_{p(XRD)}$ [nm]	16	25	13	20

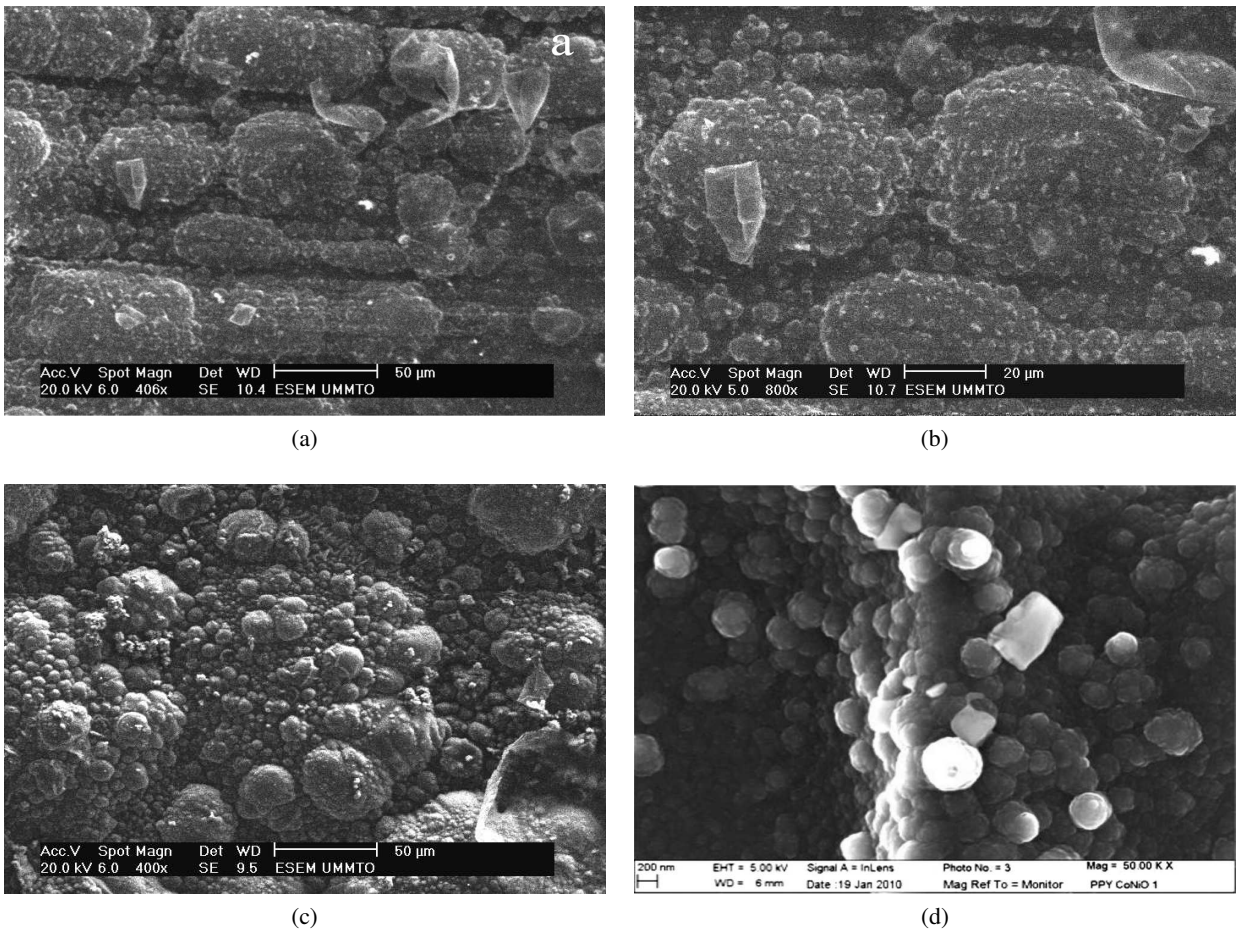

Figure 6. SEM micrographs of GC/PPy (a, b) and hybrid electrode GC/PPy/PPy($Ni_{0.3}Co_{2.7}O_4$) (c, d)

3.2. Characterization of composite electrode

The smallest $Ni_{0.3}Co_{2.7}O_4$ nanoparticles obtained with citric acid and calcined at 300 °C were selected for preparation of composite electrode. All three electrodeposition steps were analysed by chronopotentiogram. Thus, Fig. 5 shows the chronopotentiograms of the electropolymerization of Py in KCl solution, under nitrogen bubbling with and without $Ni_{0.3}Co_{2.7}O_4$ particles. The chronopotentiometric curves of Py (steps *i*, *iii*) are characterized by decrease of the potential during which the electrode is covered with a PPy layer. The succeeding plateau refers to further polymerization on already formed polymer [28]. The same plateau was reached during the formation of PPy($Ni_{0.3}Co_{2.7}O_4$) on GC/PPy (step *ii*), however the initiation stage is characterized by an increasing electrode potential. This could indicate that the presence of nanoparticles could facilitate PPy formation [29].

Morphology of the hybrid composite films was investigated by SEM (Fig. 6). SEM images of the PPy film (Figs. 6a,b) and nanocomposite film (PPy/PPy($Ni_{0.3}Co_{2.7}O_4$) (Figs. 6c,d) show a typical, the so called "cauliflower" structure as reported in literature [30]. It can be seen that $Ni_{0.3}Co_{2.7}O_4$ nanoparticles aggregates are inhomogeneously dispersed on the surface of the latter film (Figs 6c,d). EDX microanalysis confirms the presence of $Ni_{0.3}Co_{2.7}O_4$ in the composite films (not shown here).

3.3. Oxygen reduction reaction on composite electrode

Static electrode: Since PPy films exhibit no significant electroanalytical activity [31], the inserted oxide particles impact toward ORR was investigated. Therefore, linear sweep voltammetry (LSV) was recorded by scanning the potential from 0.2 to −0.8 V vs. Ag/AgCl with a rate of 5 mV/s. Three different experimental conditions were explored, i.e. aerated, deaerated, and oxygen saturated solutions (Fig. 7). It can be seen that in the absence of oxygen, no significant current densities

Table 2. The atomic Co/Ni ratio in the oxides type obtained with different chelating agents and calcined at 350 °C for 2 h

	Ni content [at.%]	Co content [at.%]
Synthesis solutions	10	90
Sample with oxalic acid	11.2	88.8
Sample with citric acid	10.46	89.54

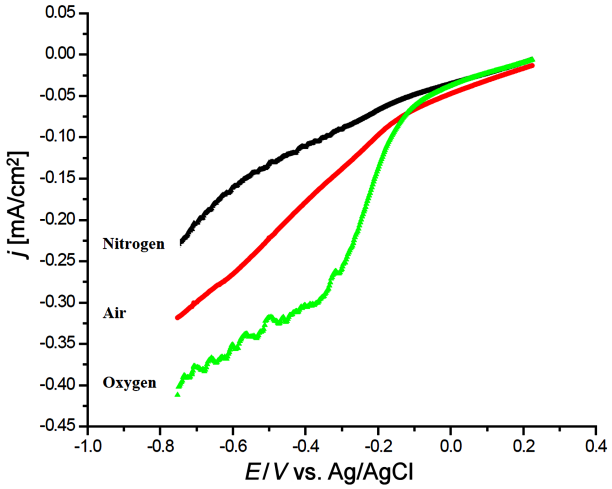

Figure 7. LSV on GC/PPy/PPy($Ni_{0.3}Co_{2.7}O_4$)/PPy electrode at 5 mV/s in a 0.15 mol/L KCl solution under nitrogen, air and oxygen atmospheres

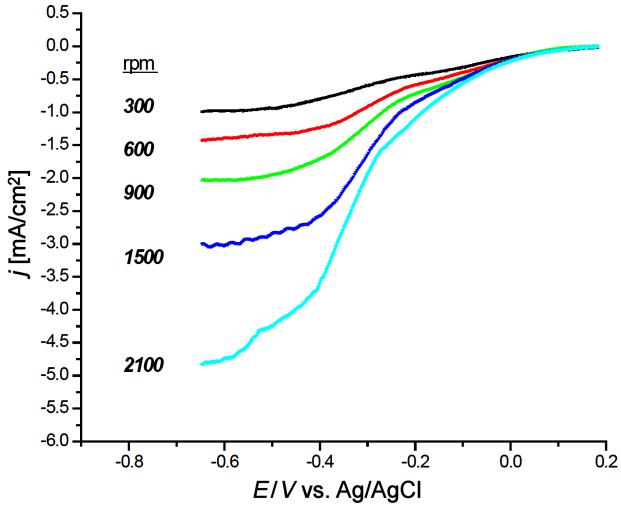

Figure 8. Polarization curves for O_2 reduction at 5 mV/s on GC/PPy/PPy($Ni_{0.3}Co_{2.7}O_4$)/PPy electrode for different rotational speeds in KCl (0.15 mol/L) O_2-saturated solution

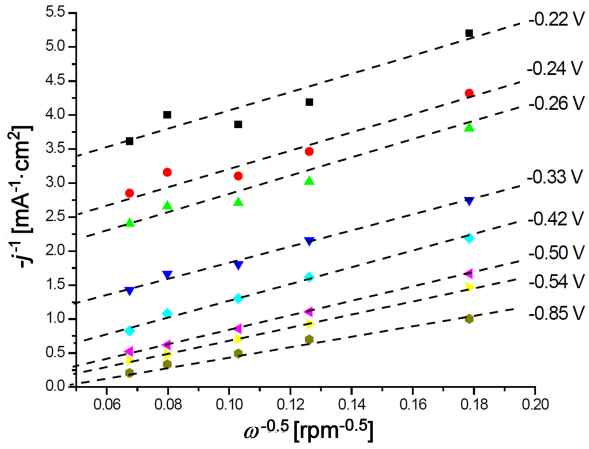

Figure 9. Koutecky-Levich (j^{-1} vs. $\omega^{-1/2}$) plots at different potentials (E)

were recorded. However, by increasing oxygen concentration, growing reduction wave was observed which confirms powder electrocatalytic activity toward ORR [27]. It was reported by Mallouki *et al.* [32] that because of polymer morphology modification, the specific charge storage capacity of the PPy(Fe_2O_3) composite electrode increase compared to the pure PPy electrode. In our case the embedded $Ni_{0.3}Co_{2.7}O_4$ nanoparticles may change the PPy film morphology and indeed, compared to the pure PPy, the composite material has finer structure and the specific surface area increases from 12 to 45 m^2/g. Nguyen Cong *et al.* [33] also obtained higher charge values for the composite electrode GC/PPy($Cu_{1.4}Mn_{1.6}O_4$)/PPy, compared to the pure PPy.

Rotating disk electrode: The obtained LSV results for the hybrid GC/PPy/PPy($Ni_{0.3}Co_{2.7}O_4$)/PPy electrode at different rotational speeds were presented in Fig. 8. As expected, the current densities are increasing with increasing the rotational speed.

Total current density j^{-1} is plotted in function of $\omega^{-1/2}$ at different potentials (Fig. 9). The straight line for each electrode potential indicate the first order reaction against dissolved oxygen [34]. Thus, for each scatter straight line, the total number of electrons n was calculated and the resulting values are reported versus electrode potentials (Fig. 10). For small applied potential (i.e. small overpotential), the total number of electrons was found to be close to $n = 2$, indicating the O_2 reduction into H_2O_2 [35]. By decreasing the applied potential (i.e. high overpotential), the total number of electrons is gradually increased up to $n = 4$. So, H_2O_2 is further reduced into H_2O. This behaviour based on potential was also reported by Chartier *et al.* [27] and attributed to a change in the mechanism with potential, which is a characteristic of the ORR on mixed valency spinel oxides.

From the K-L plot (Fig. 9), the ordinate-intercepts ($\omega \to \infty$) give the inverse of the kinetic current density for each potential. The limiting current density j_i was obtained from Fig. 11 while the parameters j_0 and

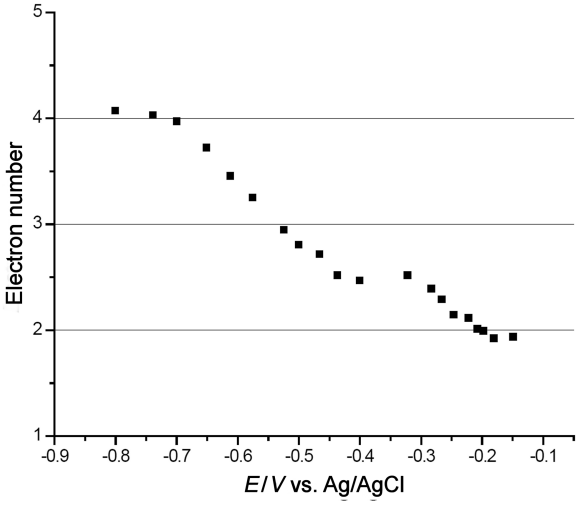

Figure 10. Variation of the total number of electrons n vs. electrode potential (E)

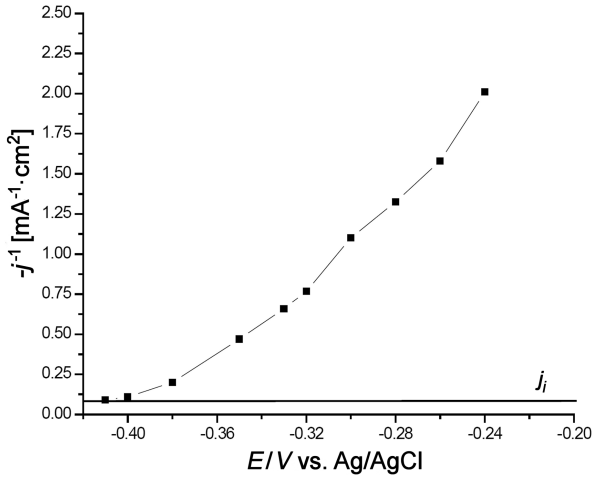

Figure 11. Plot of j^{-1} vs. E (electrode potential)

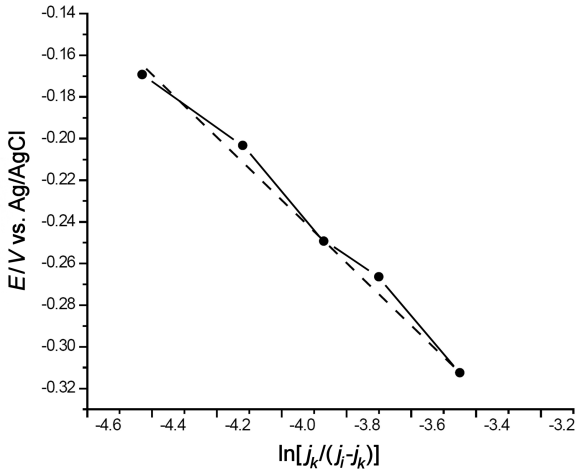

Figure 12. Plot of electrode potential (E) vs. $\ln(j_k/(j_i - j_k))$

Table 3. Kinetic parameters of ORR on GC/PPy/PPy($Ni_{0.3}Co_{2.7}O_4$)/PPy

j_i [mA/cm^2]	j_0 [mA/cm^2]	β
31	8.18×10^{-3}	0.33

β are deduced from the curve $E = f(\ln(j_k/(j_i - j_k)))$ (Fig. 12) and summarized in Table 3.

IV. Discussion

The j_0 value is 4 times higher than that reported by Chartier *et al.* [15] for the $Ni_xCo_{3-x}O_4$ having particle size of about 35 nm and obtained by thermal decomposition method. So, it seems that the sol-gel nanoparticles, due to their smaller size, exhibit better electrocatalytic activity toward ORR. Chen *et al.* [36] reported the same catalyst behaviour and suggested that Au nanoparticles exhibit much higher coordination number of the surface atoms, which promote O_2 adsorption. Therefore, its surface becomes more active. In fact, oxygen adsorption on catalyst is the first step in the electroreduction process and consequently it is more efficient when its surface allows adsorption of higher amount of oxygen [37]. Recent theoretical studies [38] have also shown that with decreasing core size of Au, the *d* bands become narrowed and shift towards the Fermi level. This finding suggests that smaller Au nanoparticles are energetically more favourable for O_2 adsorption.

As the electrocatalysis depends on both geometrical and electronic factors previously exposed, the former are those related to the extension of the actual surface area or actual site density. The latter one is that related to the surface electrical conductivity. Thus, the enhanced catalytic activity observed in our study may be ascribed, at least in part, to the $Ni_{0.3}Co_{2.7}O_4$ particle size which is smaller (higher surface area), or to its conductivity improvement.

V. Conclusions

In the present study, spinel $Ni_{0.3}Co_{2.7}O_4$ nanoparticles were successfully synthesized using sol-gel route. Particle sizes ranging from 13 to 25 nm were achieved with two chelating agents and calcination temperatures of 300 and 350 °C. The characteristic XRD peaks and the EDX peaks of Ni, Co and O confirmed the formation of the pure spinel $Ni_{0.3}Co_{2.7}O_4$ structure. Moreover, particle sizes depend more on calcination temperature than on the chelating agent, however its specific surfaces area and morphologies depend on both synthesis parameters.

The powder with the smallest particles was used to form hybrid electrode (PPy($Ni_{0.3}Co_{2.7}O_4$) film sandwiched between two PPy layers on glassy carbon. The investigation of the hybrid electrode confirmed that O_2 reduction mechanism changes by applying potential. Indeed, ORR involves two electrons to form H_2O_2, with cathodic transfer coefficient equals 0.33 and exchange current density of about 8×10^{-3} mA/cm^2 at small overpotentials. Therefore, compared to thermal decomposition, sol-gel method is considered as interesting and promising method. It enabled us to obtain fine nanoparticles, with large specific surface area and high electrocatalytic activity. It produced a larger amount of H_2O_2 making it promising for many environmental applications, including electrochemical treatment involving oxygen reduction reaction.

References

1. M.K. Carpenter, T.E. Moylan, R.S. Kukreja, M.H. Atwan, M.M. Tessema, "Solvothermal synthesis of platinum alloy nanoparticles for oxygen reduction electrocatalysis", *J. Am. Chem. Soc.*, **134** [20] (2012) 8535–8542.
2. P.E. Williams, S.T. Jones, Z. Walsh, E.A. Appel, E.K. Abo-Hamed, O.A. Scherman, "Synthesis of conducting polymer-metal nanoparticle hybrids exploiting RAFT polymerization", *ACS Macro Lett.*, **4** [2] (2015) 255–259.
3. C. Satheeshkumar, J.-Y. Park, D.-C. Jeong, S.G. Song, J. Leeb, C. Song, "Synthesis and electronic properties of N-heterocyclic carbene-containing

conducting polymers with coinage metals", *RSC Adv.*, **5** [75] (2015) 60892–60897.
4. S. Khilari, S. Pandit, D. Das, D. Pradhan, "Manganese cobaltite/polypyrrole nanocomposite-based air-cathode for sustainable power generation in the single-chambered microbial fuel cells", *Biosens. Bioelectron*, **54** (2014) 534–540.
5. R.V. Ingle, S.A. Arote, M.B. Rajendra-Prasad, V.S. Kadam, R.S. Mane, Inamuddin, Mu. Naushad, V.A. Tabhane, H.M. Pathan, "Studies on facile synthesis of polyaniline/cadmium sulfide composites and their morphology", *High Perform. Polym.*, **26** [6] (2014) 660–665.
6. Y. Shao, H.N. Cong, "Oxygen reduction on high-area carbon cloth-supported oxide nanoparticles/polypyrrole composite electrodes", *Solid State Ionics*, **178** [23-24] (2007) 1385–1389.
7. P.M. George, A.W. Lyckman, D.A. LaVan, A. Hegde, Y. Leung, R. Avasare, C. Testa, P.M. Alexander, R. Langer, M. Sur, "Fabrication and biocompatibility of polypyrrole implants suitable for neural prosthetics", *Biomater.*, **26** [17] (2005) 3511–3519.
8. X. Yuan, X.-L. Ding, C.-Y. Wang, Z.-F. Ma, "Use of polypyrrole in catalysts for low temperature fuel cells", *Energy Environ. Sci.*, **6** [4] (2005) 1105–1124.
9. L.-X. Wang, X.-G. Li, Y.-L Yang, "Preparation, properties and applications of polypyrroles", *React. Funct. Polym.*, **47** [2] (2001) 125–139.
10. F.W. Zeng, X.X. Liu, D. Diamond, K.T. Lau, "Humidity sensors based on polyaniline nanofibres", *Sensor. Actuat. B: Chem.*, **143** [2] (2010) 530–534.
11. Z.A. ALOthman, M.M. Alam, Mu. Naushad, R. Bushra, "Electrical conductivity and thermal stability studies on polyaniline Sn(IV) tungstomolybdate nanocomposite cation-exchange material: Application as Pb(II) ion-selective membrane electrode", *Int. J. Electrochem. Sci.*, **10** [3] (2015) 2663–2684.
12. M.R. Miah, T. Ohsaka, "Two-step four-electron reduction of molecular oxygen at iodine-adatoms-modified gold electrode in alkaline media", *Int. J. Electrochem. Sci.*, **7** [1] (2012) 697–710.
13. H. Wang, Y. Poya, X. Chen, T. Jia, X. Wang, J. Shi, "Hydrogen peroxide as an oxidant in starch oxidation using molybdovanadophosphate for producing a high carboxylic content", *RSC Adv.*, **5** [57] (2015) 45725–45730.
14. E. Rios, H. Nguyen-Cong, J.F. Marco, J.R. Gancedo, P. Chartier, J.L. Gautier, "Indirect oxidation of ethylene glycol by peroxide ions at $Ni_{0.3}Co_{2.7}O_4$ spinel oxide thin film electrodes", *Electrochim. Acta*, **45** [27] (2000) 4431–4440.
15. H. Nguyen-Cong, V. de la Garza Guadarrama, J.L. Gautier, P. Chartier, "$Ni_xCo_{3-x}O_4$ mixed valence oxide nanoparticles/polypyrrole composite electrodes for oxygen reduction", *J. New Mater. Electrochem. Syst.*, **5** [1] (2002) 35–40.
16. W. Tang, H. Lin, A. Kleiman-Shwarscte, G.D. Stucky, E.W. McFarland,"Size-dependent activity of gold nanoparticles for oxygen electroreduction in alkaline electrolyte", *J. Phys. Chem. C*, **112** [28] (2008) 10515–10519.
17. A. Sarapuu, M. Nurmik, H. Mändar, A. Rosental, T. Laaksonen, K. Kontturi, D.J. Schiffrin, K. Tammeveski, "Electrochemical reduction of oxygen on nanostructured gold electrodes", *J. Electroanal.Chem.*, **612** [1] (2008) 78–86.
18. S. Palmas, F. Ferrara, A. Vacca, M. Mascia, A.M. Polcaro, "Behavior of cobalt oxide electrodes during oxidative processes in alkaline medium", *Electrochim. Acta*, **53** [2] (2007) 400–406.
19. M. Hamdani, R.N. Singh, P. Chartier, "Co_3O_4 and co-based spinel oxides bifunctional oxygen electrodes", *Int. J. Electrochem. Sci.*, **5** [4] (2010) 556–577.
20. O. Parkhomey, N. Pinchuk, O. Sych, T. Tomila, O. Kuda, H. Tovstonoh, V. Gorban, V. Kolesnichenko, Y. Evych, "Effect of particle size of starting materials on the structure and properties of biogenic hydroxyapatite/glass composites", *Process. Appl. Ceram.*, **10** [1] (2016) 1–8.
21. M. Fu, Y. Lia, S. Wu, P. Lu, J. Liu, F. Dong, "Sol-gel preparation and enhanced photocatalytic performance of Cu-doped ZnO nanoparticles", *Appl. Surf. Sci.*, **258** [4] (2011) 1587–1591.
22. M. De Koninck, S.-C. Poirier, B. Marsan, "$Cu_xCo_{3-x}O_4$ used as bifunctional electrocatalyst: Physicochemical properties and electrochemical characterization for the oxygen evolution reaction", *J. Electrochem. Soc.*, **153** [11] (2006) A2103–A2110.
23. W. Xing, G. Yin, J. Zhang, *Rotating electrode methods and oxygen reduction electrocatalysts*, Elsevier, Oxford, UK, 2014
24. M. Geng, Z. Duan, "Prediction of oxygen solubility in pure water and brines up to high temperatures and pressures", *Geochim. Cosmochim. Acta*, **74** [19] (2010) 5631–5640.
25. L.-K. Ju, C.S. Ho, "Measuring oxygen diffusion coefficients with polarographic oxygen electrodes: I. Electrolyte solutions", *Biotechnol. Bioeng.*, **27** [10] (1985) 1495–1499.
26. P. Gajendran, R. Saraswathi, "Enhanced electrochemical growth and redox characteristics of poly(o-phenylenediamine) on a carbon nanotube modified glassy carbon electrode and its application in the electrocatalytic reduction of oxygen", *J. Phys. Chem. C*, **111** [30] (2007) 11320–11328.
27. H. Nguyen-Cong, V. de la Garza Guadarrama, J.L. Gautier, P. Chartier, "Oxygen reduction on $Ni_xCo_{3-x}O_4$ spinel particles/polypyrrole composite electrodes: hydrogen peroxide formation", *Electrochim. Acta*, **48** [17] (2003) 2389–2395.
28. S. Aeiyach, B. Zaid, P.C. Lacaze, "A one-step electrosynthesis of PPy films on zinc substrates by anodic polymerization of pyrrole in aqueous solution", *Electrochim. Acta*, **44** [17] (1999) 2889–2898.

29. P. Montoya, F. Jaramillo, J. Calderón, S.I.C. de Torresi, R. Torresi, "Effect of the incorporation of magnetite particles in polypyrrol films", *Portug. Electrochim. Acta*, **27** [3] (2009) 337–344.
30. J. Zhu, Y. Xu, J. Wang, J. Wang, Y. Bai, X. Du, "Morphology controllable nano-sheet polypyrrole-graphene composites for high-rate supercapacitor", *Phys. Chem. Chem. Phys.*, **17** [30] (2015) 19885–19894.
31. Q. Li, C. Zhang, J. Li, "Photocatalysis and wave-absorbing properties of polyaniline/TiO_2 microbelts composite by in-situ polymerization method", *Appl. Surf. Sci.*, **257** [3] (2010) 944–948.
32. M. Mallouki, F. Tran-Van, C. Sarrazin, C. Chevrot, J.F. Fauvarque, "Electrochemical storage of polypyrrole-Fe_2O_3 nanocomposites in ionic liquids", *Electrochim. Acta*, **54** [11] (2009) 2992–2997.
33. H. Nguyen-Cong, K. El Abbassi, J.L. Gautier, P. Chartier, "Oxygen reduction on oxide/polypyrrole composite electrodes: Effect of doping anions", *Electrochim. Acta*, **50** [6] (2005) 1369–1376.
34. W. Chen, J. Kim, S. Sun, S. Chen, "Electrocatalytic reduction of oxygen by FePt alloy nanoparticles", *J. Phys. Chem. C*, **112** [10] (2008) 3891–3898.
35. V.G. Khomenko, V.Z. Barsukov, A.S. Katashinskii, "The catalytic activity of conducting polymers toward oxygen reduction", *Electrochim. Acta*, **50** [7-8] (2005) 1675–1683.
36. W. Chen, S. Chen, "Oxygen electroreduction catalyzed by gold nanoclusters: Strong core size effects", *Angew. Chem. Int. Ed.*, **48** [24] (2009) 4386–4389.
37. J.J. Pireaux, M. Liehr, P.A. Thiry, J.P. Delrue, R. Caudano, "Electronspectroscopic characterization of oxygen adsorption on gold surfaces: I. Substrate impurity effects on molecular oxygen adsorption in ultra high vacuum", *Surf. Sci.*, **141** [1] (1984), 211–220.
38. J.A. van Bokhoven, J.T. Miller, "*d* Electron density and reactivity of the *d* band as a function of particle size in supported gold catalysts", *J. Phys. Chem. C*, **111** [26] (2007) 9245–9249.